Heliyon 10 (2024) e33923

Contents lists available at ScienceDirect

Heliyon

journal homepage: www.cell.com/heliyon

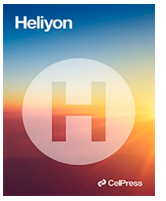

Research article

Leaching behavior and compressive strength in the immobilization of Cs-137 contaminated electric arc furnace dust via doping with activated carbon

Sudarat Issarapanacheewin [a,*], Dechanun Choomjun [a], Witsanu Katekaew [a], Nikom Prasertchiewchan [a], Wilasinee Kingkam [b]

[a] *Radioactive Waste Management Center, Thailand Institute of Nuclear Technology (Public Organization), Ongkharak, Nakhon Nayok, 26120, Thailand*

[b] *Nuclear Technology Research and Development Center, Thailand Institute of Nuclear Technology (Public Organization), Ongkharak, Nakhon Nayok, 26120, Thailand*

ARTICLE INFO

Keywords:
Electric arc furnace dust
Cs-137
Activated carbon
Compressive strength
Leaching behavior

ABSTRACT

This study evaluated the potential of an immobilization technique to inhibit the migration and dispersion of Cs-137 contaminated electric arc furnace dust (EAFD) into the environment, by investigating its compressive strength and leaching characteristics. The EAFD was employed to replace ordinary Portland cement (OPC) in varied ratios, ranging from 0 % to 50 % by weight. The replacement was done using various water-binder ratios of 0.35, 0.40, 0.45, and 0.50. Furthermore, the use of activated carbon (AC) has been shown to minimize radionuclide and heavy metal discharge related to its high porosity. AC was added at weight concentrations of 0.5 %, 1.0 %, 1.5 %, and 2.0 %. Compressive strength and leaching tests are used to assess the long-term stability of waste forms and the effectiveness of immobilizing radioactive wastes, which is beneficial for storing and disposing of radioactive waste. The compressive strength is affected by the amount of EAFD, water-to-binder ratios, the addition of AC, and the duration of curing. Measurements of specific surface area, pore size, pore volume, and porosity were also carried out under various conditions. The research results indicate that the addition of AC improves the compressive strength and decreases the release of Cs-137 and heavy metals from the specimen. The mixture of 45 % EAFD and 1.5 % AC is appropriate for efficiently immobilizing Cs-137 contaminated EAFD.

1. Introduction

The steel industry is predominantly produced on electric arc furnace (EAF) technology. Scrap metals are the primary raw materials used to manufacture steel. Electric arc furnace dust (EAFD) is a byproduct of the high-temperature scrap metal recycling process. The scrap metals were graded and melted in the EAF. Upon completion of the smelting process, the EAFD is collected through a capture system by using a filter bag [1,2]. EAFD is a hazardous waste due to the presence of heavy metals such as iron (Fe), zinc (Zn), lead (Pb), chromium (Cr), aluminum (Al), and manganese (Mn), which are detrimental effects on human health and the environment [2–5].

* Corresponding author.
E-mail address: sudarat@tint.or.th (S. Issarapanacheewin).

https://doi.org/10.1016/j.heliyon.2024.e33923
Received 8 April 2024; Received in revised form 24 June 2024; Accepted 30 June 2024
Available online 1 July 2024

Additionally, radioactive contamination with cesium-137 (Cs-137) was founded in EAFD. This is classified as radioactive waste because it exceeds the legal limit for radioactivity. In general, EAFD waste is typically incinerated or sent to a landfill for disposal. However, when EAFD becomes radioactive waste, it must be properly managed so that it does not negatively impact people or the environment [3–7]. The classification of radioactive wastes includes various categories based on their level of radioactivity and half-life. These categories are known as very short-lived waste (VSLW), very low-level waste (VLLW), low-level waste (LLW), intermediate-level waste (ILW), and high-level waste (HLW) [8,9].

Immobilization is the process of transforming radionuclides into a stable solid form through stabilization and solidification to prevent the waste from migrating or dispersing into the environment, thereby making it suitable for transport, storage, and final disposal. The immobilization technology can be processed in a variety of methods, including cementation, bituminization, vitrification, and polymerization [10–12]. Cementation has been utilized for the immobilization of low and intermediate level radioactive waste, including Cs-137, which has a half-life of approximately 30.17 years [13,14]. Ordinary Portland Cement (OPC) is an appropriate matrix material as a primary binder that stabilizes the retention of radionuclides in the matrix and enhances mechanical performance. In addition, fly ash, blast furnace slag, electric arc furnace dust, bentonite, zeolite, activated carbon, and other materials were used as binders in order to improve the mechanical performance [15–17]. The assessment of compressive strength is used to evaluate the long-term stability of waste forms that are beneficial for the storage of radioactive waste and the disposal of radioactive waste in its ultimate state. In order for radioactive cement waste forms to be stored for an extended period of time, the mechanical strength criteria must be more than 3.45 MPa, which is equivalent to 34.5 kg·f/cm^2. Moreover, the quantity of radionuclides that are released from a waste form may be determined with the use of the leaching test [18–21].

Cement-based EAFD waste form has to be in solid form and resistant to leaching before being disposed of, hence compressive strength and leaching behavior were studied [20,21]. Activated carbon (AC) is being evaluated for use in the construction of anti-migration barriers for radionuclides and heavy metals because of its high sorption capacity. Activated carbon was thus added to the cement-based EAFD in order to improve the rate at which radionuclides and heavy metals were adsorbed during the leaching test. This was accomplished without a reduction in the compressive strength of the material [22].

2. Background research

In 2018, the steel manufacturing factory discovered over 880 tons of EAFD contaminated with the radioactive Cs-137. The radioactivity levels of EAFD vary between 0.42 and 486.68 Bq/g [9]. These values are much higher than the threshold of 0.1 Bq/g, as indicated in the Ministerial Regulation on Radioactive Waste Management, B.E. 2561, 2018. Consequently, EAFD is categorized as low-level radioactive waste (LLW) due to its activity concentration and half-life. Experiments are being conducted on a small scale in a laboratory to decrease the amount of radioactivity in the EAFD using extraction and co-precipitation methods [23–25]. In addition, waste conditioning is performed to handle the contaminated EAFD. In this study, our main objective is to immobilize EAFD using the

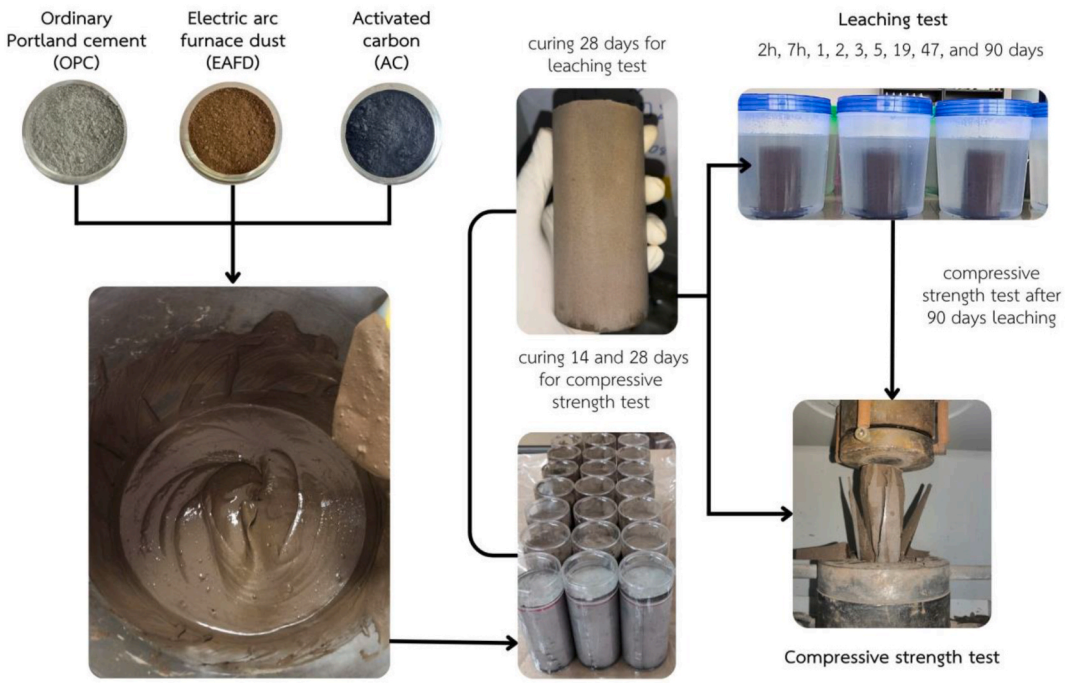

Fig. 1. The procedure for evaluating the compressive strength and leaching characteristics in the immobilization of Cs-137 contaminated Electric Arc Furnace Dust (EAFD).

cementation approach because of its exceptional mechanical properties, cost-effectiveness, and simple operation.

3. Significance of the investigation

Thailand is currently confronting an issue with EAFD contaminated with the radioisotope Cs-137. They are categorized as radioactive waste as it exceeds the radioactivity threshold. Cementation has been used to immobilize radioactive waste to limit their migration and dispersion into the environment, making it safe for transportation and long-term storage. Compressive strength and leaching tests evaluate the long-term stability of waste forms and the efficiency of immobilizing radioactive wastes. Furthermore, activated carbon (AC) was added to the waste form to improve the compressive strength and to minimize the release of radionuclides and heavy metals. Fig. 1 displays the process diagram for producing the OPC-based EAFD specimen and performing compressive strength and leaching tests. The research findings could potentially be applied to managing EAFD contaminated with Cs-137. This study involved the characterization of Cs-137-contaminated EAFD as a form of radioactive waste. Subsequently, the EAFD was subjected to treatment through immobilization using OPC via the process of cementation. When evaluating long-term disposal alternatives, it is imperative to consider factors such as waste loading, compressive strength, and resistance to radionuclide leaching.

4. Materials and test methods

4.1. Materials

Ordinary Portland cement (OPC), ASTM C150 Type 1, was procured from TPI Polene (Public) Co., Ltd. This cement was used to immobilize electric arc furnace dust (EAFD) contaminated with Cs-137, originating from the steel manufacturing industry. The immobilized addition was carried out using activated carbon (AC), purchased from DC Fine Chemicals. The physical appearance of EAFD, OPC, and AC are shown in Fig. 1. The EAFD, OPC, and AC are characterized by their appearance as brown powder with varying sizes, grey homogenous powder, and black fine powder, respectively. The bulk density of OPC, EAFD, and AC is approximately 1.01 g/cm^3, 0.83 g/cm^3, and 0.32 g/cm^3, respectively.

The XRF method was used to study the chemical composition of all materials, and the findings are shown in Table 1. The major compounds found in EAFD are zinc oxide (ZnO) and iron(III) oxide (Fe_2O_3), whereas the main chemical composition of OPC is calcium oxide (CaO).

4.2. Mixing and sample preparation

Cementitious materials were produced by mixing EAFD and OPC, with varying amounts of EAFD replacing OPC, ranging from 0 % to 50 %. The water-to-binder ratio (w/b) was manipulated at values of 0.35, 0.40, 0.45, and 0.50. The addition of AC was implemented in OPC-based EAFD at varying weight percentages, namely 0.5 %, 1.0 %, 1.5 %, and 2.0 %. Table 2 shows mixed proportion of all samples. In the first step, a combination of OPC, AC, and EAFD was mixed and left to blend for a period of 5 min. Following the attainment of homogeneity, tap water was subsequently incorporated into the mixture and subjected to blending for 5 min.

Table 1
The chemical composition of electric arc furnace dust (EAFD), ordinary Portland cement (OPC), and the replacement of EAFD ranges from 0 % to 50 % by weight.

Compound	Concentration (wt%)							
	EAFD	OPC	15%EAFD	25%EAFD	35%EAFD	40%EAFD	45%EAFD	50%EAFD
ZnO	36.69 %	0.03 %	6.60 %	11.85 %	16.01 %	17.73 %	20.09 %	21.52 %
Fe_2O_3	34.43 %	3.67 %	9.02 %	13.70 %	16.73 %	17.68 %	19.23 %	20.96 %
Cl	7.21 %	0.27 %	0.62 %	1.02 %	1.43 %	1.51 %	2.37 %	2.19 %
SiO_2	3.58 %	16.27 %	14.86 %	10.85 %	9.18 %	8.63 %	9.27 %	8.25 %
CaO	3.18 %	69.99 %	58.77 %	52.65 %	46.90 %	44.75 %	37.41 %	35.13 %
K_2O	2.83 %	0.53 %	1.17 %	1.78 %	2.36 %	2.00 %	2.73 %	2.19 %
SO_3	2.80 %	3.74 %	2.19 %	2.05 %	1.71 %	1.90 %	2.36 %	2.10 %
MgO	2.77 %	1.41 %	1.38 %	1.03 %	1.09 %	1.10 %	1.35 %	1.21 %
MnO	2.45 %	0.05 %	0.50 %	0.81 %	1.03 %	1.14 %	1.27 %	1.39 %
PbO	1.83 %	–	0.34 %	0.66 %	0.89 %	0.94 %	1.09 %	1.18 %
Al_2O_3	0.80 %	3.38 %	2.94 %	2.13 %	1.95 %	1.82 %	2.01 %	1.97 %
Cr_2O_3	0.42 %	–	0.08 %	0.12 %	0.16 %	0.21 %	0.21 %	0.25 %
P_2O_5	0.29 %	0.10 %	–	0.79 %	–	–	–	1.07 %
Br	0.26 %	–	0.03 %	0.07 %	0.09 %	0.10 %	0.13 %	0.13 %
CuO	0.25 %	0.03 %	0.06 %	0.09 %	0.12 %	0.13 %	0.14 %	0.16 %
TiO_2	0.11 %	0.31 %	0.33 %	0.31 %	0.29 %	0.30 %	0.26 %	0.22 %
CdO	0.03 %	–	–	–	–	–	–	–
NiO	0.02 %	0.01 %	0.01 %	0.02 %	0.02 %	0.01 %	0.02 %	0.02 %
Rb_2O	0.02 %	–	–	–	–	0.01 %	0.02 %	0.02 %
Na_2O	–	0.14 %	1.05 %	–	–	–	–	–
SrO	–	0.04 %	0.04 %	0.04 %	0.04 %	0.04 %	0.03 %	0.03 %

Table 2
Mixed proportion of all samples for compressive strength, leaching, and porosity tests.

w/b ratio	EAFD (%)	OPC (%)	AC (%)	Curing time (days)	Curing temperature
0.35	0	100	–	14 and 28	Room temp.
0.40	15	85			
0.45	25	75			
0.50	35	65			
	40	60			
	45	55			
	50	50			
0.40	0	100	0.5		
	15	85	1.0		
	25	75	1.5		
	35	65	2.0		
	40	60			
	45	55			
	50	50			

Subsequently, the mixture was carefully inserted into cylindrical plastic molds, which possessed a diameter of 5 cm and a height of 10 cm. The curing process for all samples was carried out at room temperature for 14 and 28 days.

4.3. Tests

4.3.1. Compressive strength test

The compressive strength test was conducted using the hydraulic press equipment (Chun Yen, CY-6690). After curing for 14 and 28 days, the cylindrical specimens with a diameter of 5 cm and a height of 10 cm were subjected to compressive strength testing. The average values of compressive strength obtained from the three repetitions were recorded. As to the U.S. Nuclear Regulatory Commission, the compressive strength requirement should exceed 3.45 MPa [26].

4.3.2. Leaching test

The leaching behavior of all specimens was evaluated after a curing period of 28 days. Leaching was tested on three cylindrical specimens measuring 5 cm in diameter and 10 cm in height. The specimen was immersed in a plastic bucket containing deionized water, with the amount of water being around 10 times the surface area of the specimens. The radioactivity of the leachate was evaluated by Gamma spectroscopy (GEM-C40, Ametek Ortec, USA) at various time intervals, including 2 h, 7 h, 1 day, 2 days, 3 days, 4 days, 5 days, 19 days, 47 days, and 90 days. The ICP-MS (Shimadzu, ICPMS-2030) determined the concentration of heavy metal and cesium ions in the leachate at the initial and after 90 days of leaching. The study investigated the leaching behavior pattern using the leach method prescribed by the International Atomic Energy Agency (IAEA). The calculation of the cumulative fraction leached (CFL) of radionuclides can be derived from Eq. (1) [27]:

$$CFL = \sum a_n \Big/ A_0 \tag{1}$$

where Σa_n is the total amount of radioactivity that has been released from the specimen and A_0 the initial radioactivity present in the specimen.

The determination of the effective diffusion coefficient (D_e) for evaluating the long-term behavior of radionuclides can be achieved by applying Fick's diffusion theory for a semi-infinite medium, as represented by Eq. (2). This calculation is specifically applicable when the CFL condition is below 20 % [8].

$$D_e = \pi \times \left\{ \left[(a_n / A_0) \,/\, (\Delta t)_n \right] exp.2 \right\} \times [(V/S) exp.2] \times T \tag{2}$$

where D_e is the determination of the effective diffusion coefficient (cm^2/s), $(\Delta t)_n$ is the cumulative time (s), V is the volume of specimen (cm^3), S is the exposed surface area of the specimen (cm^2), and T is the leaching period for a semi-infinite medium (s), can be determined using Eq. (3) [8].

$$T = \{1/2 \times [(t_n) exp.1/2 + (t_n) exp.1/2]\} exp.2 \tag{3}$$

If the CFL exceeds 20 %, the D_e can be determined using Eq. (4), where G is the dimensionless time factor for the specimen, as determined by the American National Standard ANSI/ANS 16.1 [28], and d is the diameter of the specimen (cm) [8].

$$D_e = [G \times (d exp.2)] / t \tag{4}$$

The leachability index (LI) refers to a material parameter that characterizes the leachability of diffusing species. It is commonly employed to assess the effectiveness of a matrix material in solidifying waste. The leachability index is mathematically represented by Eq. (5) [8,29].

$$LI = 1 \log D_e \quad (5)$$

A threshold value of 6 or higher is considered acceptable for determining the adequacy of a given matrix in immobilizing radioactive wastes.

4.3.3. Porosity test

The porosity was measured using the Archimedes method, following the ASTM C20-00 testing methodology. The cylindrical specimens were prepared with a diameter of 3 cm and a height of 3 cm, then cured for 28 days. After that, the samples were dried in an oven at a temperature of 100 °C for 24 h. The dry weight (D) of each specimen was measured. Subsequently, the specimens were placed into a boiling water at a temperature of 100 °C for 2 h. The specimens were cooled in the water until they reached the ambient temperature. The suspended weight (S) was measured by submerging them in water and using a copper wire attached to a balance. The specimens were removed any moisture on the surface and then their saturated weight (W) was measured. The calculation of apparent porosity in percentage (P) was performed using Eqs. (6) and (7) [17]:

$$P = [(X - D) / V] \times 100 \quad (6)$$

$$V = W - S \quad (7)$$

where W is the saturated weight, D is the dry weight, S is the suspended weight, and V is the exterior volume of the specimen.

4.4. Characterization

The crystal structure of all specimens was determined using X-ray diffraction (XRD) using a Bruker D8 ADVANCE instrument. The scanning electron microscopy-energy dispersive X-ray spectroscopy (SEM-EDS) technique was used to examine the surface morphology, microstructure, size, and element composition. The Hitachi Model SU5000 was used for this investigation. The chemical composition was examined using X-ray fluorescence (XRF) using the Bruker S8 Tiger model. The nitrogen (N_2) adsorption-desorption isotherm was obtained using a Micromeritics 3Flex physisorption analyzer. The specimens underwent degassing at 60 °C for 3 h in a vacuum environment to remove moisture from the specimen. The specific surface area was determined using the Brunauer-Emmett-Teller (BET) method, which relies on the N_2 adsorption isotherm. The Barrett-Joyner-Halenda (BJH) method was used to evaluate the pore sizes distribution in the desorption region of the N_2 adsorption-desorption isotherm.

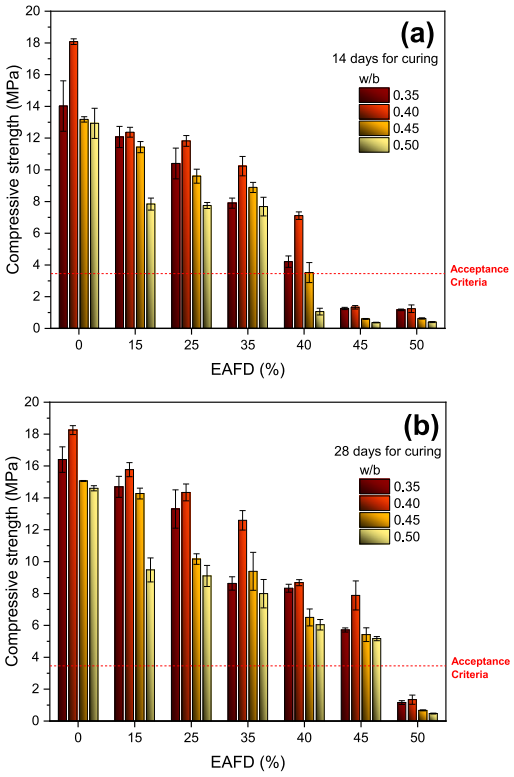

Fig. 2. The compressive strength of all specimens at various concentrations of EAFD, water-to-binder (w/b) ratios of 0.35, 0.40, 0.45, and 0.50, and two different curing periods: (a) 14 days and (b) 28 days.

5. Results and discussion

5.1. Compressive strength

Fig. 2 displays the compressive strength data of the specimens at various EAFD replacement after a curing period of 14 and 28 days. The specimens were subjected to different water-to-binder (w/b) ratios, specifically 0.35, 0.40, 0.45, and 0.50. The results suggest that there is a clear decrease in the compressive strength as the amount of EAFD replacement rises. The decrease in compressive strength found in this research may be attributed to the comparatively low concentrations of CaO and SiO_2. These two compounds are essential for the formation of the calcium silicate hydrates (C–S–H) gel that is produced during the hydration process (Eq. (8) and Eq. (9)). The C–S–H gel is recognized for its significant contribution to the strength of the cement-based materials [30,31]. The decrease in strength can additionally be ascribed to the interaction between Zn in EAFD and calcium hydroxide ($Ca(OH)_2$), resulting in the formation of calcium hydroxyzincate hydrate ($CaZn_2(OH)_6{\cdot}2H_2O$), as seen in Eq. (10), which hinders the hydration process [32,33].

$$2(3CaO{\cdot}SiO_2) + 6H_2O \rightarrow 3CaO{\cdot}2SiO_2{\cdot}3H_2O + 3Ca(OH)_2 \quad (8)$$

$$2(2CaO{\cdot}SiO_2) + 4H_2O \rightarrow 3CaO{\cdot}2SiO_2{\cdot}3H_2O + Ca(OH)_2 \quad (9)$$

$$2ZnO + Ca(OH)_2 + 4H_2O \rightarrow CaZn_2(OH)_6{\cdot}2H_2O \quad (10)$$

Fig. 2 demonstrates that extending the curing time from 14 to 28 days increases the compressive strength of all materials. The compressive strength of all specimens after 14 days of curing, with a w/b ratio of 0.40, is assessed. The values obtained are 18.08, 12.37, 11.82, 10.23, 7.11, 1.33, and 1.24 MPa for 0 %, 15 %, 25 %, 35 %, 40 %, 45 %, and 50 % of EAFD replacement, respectively. Following the curing time of 28 days, the compressive strength of the material improves to 18.25, 15.77, 14.34, 12.59, 8.68, 7.88, and 1.34 MPa for 0 %, 15 %, 25 %, 35 %, 40 %, 45 %, and 50 % of EAFD replacement, respectively. The occurrence may be elucidated by the ongoing hydration reaction that takes place while the curing process is underway. The process of curing significantly influences the properties of concrete since it has a dramatic impact on the hydration of cement. Efficient curing facilitates the ideal environment for the formation of hydration products, leading to a reduction in porosity and an increase in the density of the microstructure in concrete [34,35].

Adjusting the water-to-binder ratios impact on the compressive strength, as observed in Fig. 2. Decreasing the ratio to 0.40 results

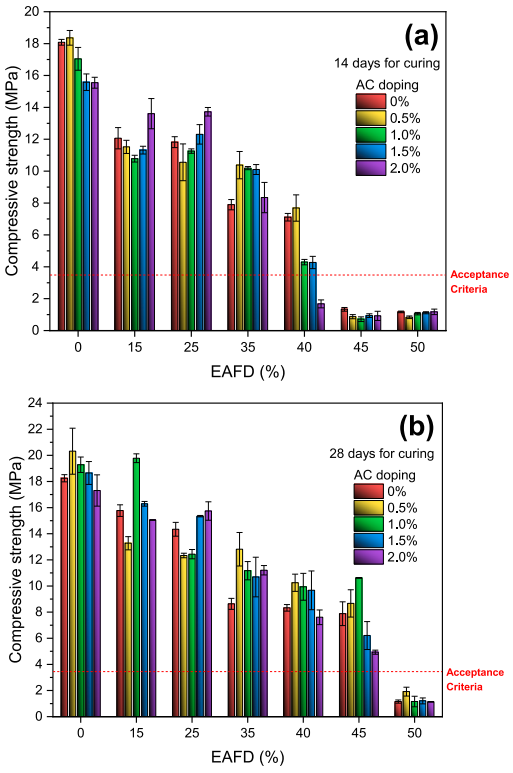

Fig. 3. The compressive strength of all specimens was measured at water-to-binder (w/b) ratios of 0.40. The specimens were doped with varied levels of activated carbon and replaced with varying amounts of EAFD. The compressive strength was tested after curing for two distinct periods: (a) 14 days and (b) 28 days.

in an enhancement in strength. However, reducing it further to 0.35 leads to a decline in compressive strength. The strength of concrete is achieved by the process of cement hydration. During the initial hydration process, the cement particles become weakly bound together, with a surrounding area filled with water. Higher water content leads to increase the spacing between cement grains. Increasing water-to-binder ratios result in the formation of interconnected pores, which consequently reduces the strength of the concrete. However, when the water-to-binder ratio is 0.35, there is an excess of cement that does not react with water during the hydration process, resulting in a loss in compressive strength [16,36].

Specimens were added with AC at weight percentages of 0.5, 1.0, 1.5, and 2.0 after being substituted with varying quantities of EAFD using water-to-binder (w/b) ratios of 0.40. The compressive strength of all specimens was measured after a curing period of 14 and 28 days, as shown in Fig. 3. These results indicate that the addition of AC enhanced the compressive strength of the specimens. Fig. 4 illustrates the porosity of all samples throughout a 28-day curing period. Fig. 4 illustrates the porosity of all samples throughout a 28-day curing. It was shown that decreasing porosity significantly improves compressive strength. AC has a large specific surface area and a microporous structure, allowing it to occupy the voids formed during the hydration process efficiently [37–39].

The specimens performed a leaching test lasting 90 days. Afterwards, the compressive strength was assessed, as shown in Table 3. Certain specimens demonstrated reduced compressive strength compared to those cured for 28 days in a dry environment. This finding suggests that the specimens were submerged in water within a wet setting, resulting in a detrimental impact and the release of the contents of the specimen [14,40]. Nevertheless, several specimens, particularly those with 45 % and 50 % EAFD replacement, exhibited significantly greater compressive strength when compared to the 28-day curing time. This enhancement may be attributed to the specimens being exposed to more water through immersion, which facilitated a continuous hydration process of the cementitious materials combined with EAFD [40,41].

5.2. Leachability

An investigation of 90 days was conducted to assess the leaching test of Cs-137, following the guidelines set by the IAEA leaching and ANSI/ANS-16.1-2003 standard. The measurement of the cumulative fraction leached (CFL) for Cs-137 is shown in Fig. 5. The study examined the leaching behavior and its impact on varying amounts of activated carbon (AC) addition. Fig. 5a and c displays the CFL of various EAFD replacements with 0 % and 1.0 % of AC addition, respectively. The CFL values range from 0.8 to 1.0 and the testing period is 90 days. However, the addition of 0.5 % by weight of AC, replacing 15 % of the EAFD, resulted in a significantly decrease in the CFL value from 0.85 to 0.74. Furthermore, the CFL value decreases slightly to 0.86 when 0.5 % AC doping is combined with 25 %, 35 %, and 40 % EAFD replacements, as shown in Fig. 5b. By increasing the AC concentration to 1.5 % by weight (Fig. 5d), the CFL value of EAFD replacements at 40 %, 45 %, and 50 % had a reduction within the range of 0.80–0.85. The CFL value exhibited a decrease to a range of 0.70–0.76 when the EAFD replacements were at 15 %, 25 %, and 35 %, as shown in Fig. 5d. Fig. 5e displays the CFL value resulting from AC doping at a concentration of 2.0 % by weight, while the EAFD replacements are varied. During the testing period of 90 days, it was noted that the CFL value of the EAFD replacement, which accounted for 15 %, reduced to 0.62.

The leachability index (LI) was calculated for all specimens and is shown in Table 4. To guarantee the effective and long-term disposal of the radioactive waste, the LI of the cemented radioactive waste form must exceed a minimum value of 6. The average LI of all specimens is between 5.72 and 7.01, indicating that some specimens, namely those composed of 35–50 % EAFD with 0 % AC, 45–50 % EAFD with 0.5–1.0 % AC, and 50 % EAFD with 1.5–2.0 % AC, are unsuitable for extended storage. The chemistry of elements

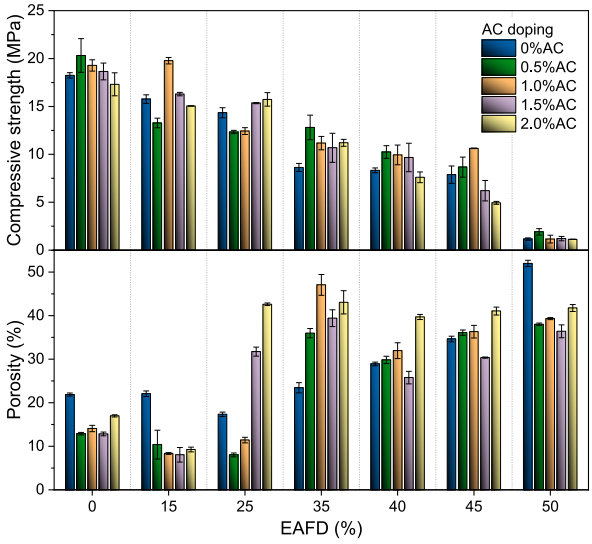

Fig. 4. The porosity and compressive strength of all specimens under different levels of EAFD and AC doping throughout a 28-day curing period, with a water-to-binder ratio of 0.40.

Table 3
The compressive strength of all specimens at various curing times.

Compressive strength (MPa)										
Samples	0%AC		0.5%AC		1.0%AC		1.5%AC		2.0%AC	
Curing time	**28 days**	**90 days**	**28 days**	**90 days**	**28 days**	**90 days**	**28 days**	**90 days**	**28 days**	**90 days**
0%EAFD	18.25	15.72	20.32	21.32	19.28	25.18	18.65	17.43	17.31	22.17
15%EAFD	15.77	10.39	13.27	17.80	19.78	15.00	16.29	13.06	15.05	16.21
25%EAFD	14.34	9.19	12.33	13.27	12.44	11.32	15.35	14.15	15.74	10.22
35%EAFD	8.63	8.06	12.81	12.83	11.17	9.02	10.69	8.32	11.21	8.68
40%EAFD	8.33	8.60	10.25	10.60	9.94	8.12	9.67	7.86	7.61	10.23
45%EAFD	7.88	11.39	8.67	11.03	10.62	11.49	6.21	7.57	4.94	7.74
50%EAFD	1.16	9.05	1.91	9.69	1.16	10.36	1.21	9.61	1.13	8.17

*90 days refers to the curing time after the leaching test.

or chemical properties may influence its leaching characteristics [42].

ICP-MS was utilized to determine the presence of cesium and heavy metal ions in the leachates from the initial and 90-day leaching periods, as shown in Table 5. The elemental composition of the initial leachate consists of Al, Cd, Cr, Cs, Cu, Fe, Mn, Ni, Pb, and Zn. Following 90 days of curing, the specimens exhibited little release of cesium and heavy metal ions. Some elements in the leachate were not detected due to their amounts being below the detection limit. It can be assumed that the variation in the amount of cesium and heavy metal ions leached may be related to their differing bonding strength within the cement matrix and solubility [8]. Furthermore, AC serves as a highly porous material that efficiently absorbs heavy metals and radionuclides. It has the potential to impact the effectiveness of barriers that prevent the migration of heavy metals and radionuclides [43].

Fig. 6 depicts the pH measurements of leachates from cemented waste forms at different time intervals, up to a maximum of 90 days. The deionized water (DI) used in the leaching examination exhibited a pH of around 5.0 when measured at ambient temperature. The leachates exhibit a pH range of 9.0–12.5 during the leaching test as a result of the dissociation of $Ca(OH)_2$ formed during the hydration process, as shown by Eqs. (8) and (9). The pH had a slight rise to about 12.1 by day 19, followed by a decrease to approximately 11.4 by day 90 due to the consumption of hydroxides during the dissociation process of $Ca(OH)_2$ [8].

5.3. XRF analysis

The chemical composition of all specimens was analyzed using an XRF spectrometer, and the findings are shown in Table 1. Zinc oxide (ZnO) and iron(III) oxide (Fe_2O_3) were found to be the main chemical components of EAFD, accounting for 36.69 % and 34.43 %, respectively. Additionally, EAFD has several heavy metal constituents, including PbO, MnO, CdO, CuO, NiO, Cr_2O_3, and Al_2O_3. The XRF analysis of the OPC revealed that its major chemical compounds were calcium oxide (CaO) and silicon oxide (SiO_2), which accounted for 69.99 % and 16.27 %, respectively. The OPC was substituted with EAFD in the ranges of 0 %–50 % by weight. This substitution resulted in different components originating from both OPC and EAFD. As the concentration of EAFD in the specimen increased, the content of ZnO and Fe_2O_3 compounds in EAFD also increased. Consequently, this caused a reduction in the concentration of CaO.

5.4. XRD analysis

The X-ray diffraction (XRD) technique was applied to ascertain the crystal structure and composition of the materials. Fig. 7 exhibits the XRD patterns of OPC, EAFD, and the replacement of EAFD at the curing time of 28 days. The main crystalline phase of OPC comprises tricalcium silicate or alite (Ca_3SiO_5) and dicalcium silicate or belite (Ca_2SiO_4). The XRD pattern of EAFD reveals the existence of two primary crystal structures, including zinc ferrite or franklinite ($ZnFe_2O_4$), and zinc oxide or zincite (ZnO). The structures of $ZnFe_2O_4$ and ZnO are classified as cubic spinel and hexagonal Wurtzite structures, respectively. Upon increasing the weight percentage of EAFD from 0 % to 50 %, the XRD analysis revealed an increase in the intensity of $ZnFe_2O_4$ and ZnO peaks. Consequently, this resulted in a drop in the XRD intensity of Ca_3SiO_5 and Ca_2SiO_4 in OPC. The XRD peak at around 17° indicates the presence of $Ca(OH)_2$, which is formed during the hydration reaction of cement, in both the OPC and the replacement of EAFD. The intensity of $Ca(OH)_2$ decreased when the amount of EAFD was reduced from 15 % to 50 %, suggesting a low quantity of $Ca(OH)_2$ in the specimen. The replacement of EAFD results in a reduction in compressive strength [32].

5.5. SEM-EDS analysis

The morphology and elemental composition of the materials were evaluated by applying the techniques of scanning electron microscopy and energy-dispersive X-ray spectroscopy (SEM-EDS). The morphology of EAFD, OPC, AC, 45 % EAFD, and a mixture of 45 % EAFD doped with 2.0 % AC is shown in Fig. 8. The morphology of EAFD is characterized by the presence of agglomerated spherical particles and smooth surfaces, with a dimension ranging from 700 to 1500 nm, as seen in Fig. 8a. The morphological features of OPC are depicted in Fig. 8b. These include smooth to rough surface particles that possess angular shapes. The dimensions of these particles vary between 5 and 20 μm in width and 10–25 μm in length. In Fig. 8c, the AC exhibits a morphology comprised of particles with a

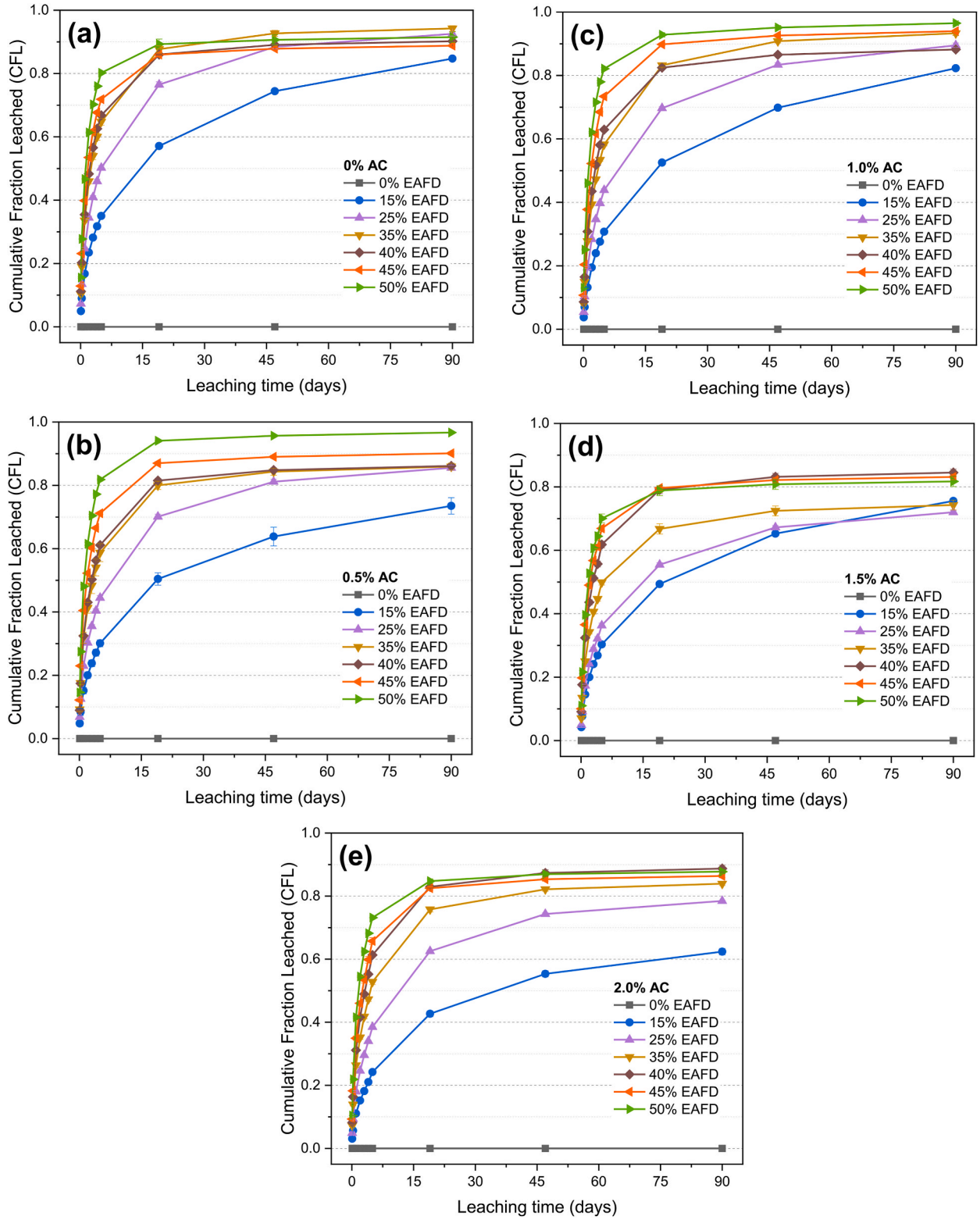

Fig. 5. The CFL of several EAFD samples with varying AC doping: (a) 0 %, (b) 0.5 %, (c) 1.0 %, (d) 1.5 %, and (e) 2.0 %.

Table 4
The leachability index (LI) of all specimens.

Samples	Leachability index, LI				
	0%AC	0.5%AC	1.0%AC	1.5%AC	2.0%AC
15%EAFD	6.48	6.70	6.75	6.75	7.01
25%EAFD	6.26	6.35	6.44	6.61	6.53
35%EAFD	6.00	6.10	6.14	6.31	6.25
40%EAFD	5.97	6.08	6.10	6.08	6.11
45%EAFD	5.86	5.88	5.94	6.02	6.03
50%EAFD	5.72	5.72	5.77	5.95	5.95

Table 5
The leachate from the initial and 90-day leaching periods was analyzed using ICP-MS to identify the presence of heavy metal and cesium ions.

Element	Ion concentration (mg/L)									
	45%EAFD		45%EAFD + 0.5%AC		45%EAFD + 1.0%AC		45%EAFD + 1.5%AC		45%EAFD + 2.0%AC	
	Initial	90 days	Initial	90 days	Initial	90 days	Initial	90 days	Initial	90 days
Al	4392.48	1.68	4266.24	1.79	4569.15	1.71	4384.76	1.69	4394.41	1.89
Cd	24.63	< DL	23.69	< DL	25.03	< DL	23.93	< DL	23.74	< DL
Cr	277.51	< DL	323.59	< DL	368.86	< DL	371.09	< DL	389.94	< DL
Cs	1.92	0.11	1.91	0.09	1.93	0.09	1.90	0.10	1.88	0.09
Cu	205.15	< DL	223.49	0.05	240.64	< DL	228.66	< DL	233.96	< DL
Fe	24,563.55	< DL	30,860.81	0.52	32,334.05	< DL	31,068.57	0.06	33,134.79	0.17
Mn	2561.89	< DL	2842.38	< DL	3085.25	< DL	2890.13	< DL	2932.25	< DL
Ni	19.63	< DL	22.92	< DL	26.95	0.06	28.87	0.06	35.04	0.10
Pb	187.06	0.23	341.93	0.17	823.58	0.15	151.55	0.32	712.43	0.24
Zn	44,347.79	< DL	46,098.86	< DL	49,895.27	< DL	46,412.19	< DL	47,862.70	0.14

*DL is the detection limit (0.05 mg/L).

smooth surface and a needle-like shape, measuring 5–12 μm in width and 20–35 μm in length.

Fig. 8d illustrates the morphology of the 45 % EAFD based on OPC with a water-to-binder ratio of 0.40 after 28 days of curing. The OPC underwent hydration reaction with water, resulting in the formation of calcium hydroxide ($Ca(OH)_2$) and calcium silicate hydrate gel (C–S–H) [12,31]. The morphology of the OPC-based 45 % EAFD consists of spherical particles of varying sizes of EAFD that adhere to the angular shape of OPC. Additionally, the surfaces of both EAFD and OPC exhibit increased roughness as a result of the deposition of hydration products on their surfaces [14,44]. Fig. 8e and f shows the morphology and elemental composition of a mixture consisting of 45 % EAFD that has been doped with 2.0 % AC, respectively. After 28 days of curing, the morphology of a mixture consisting of 45 % EAFD doped with 2.0 % AC and a water-to-binder ratio of 0.40 comprises agglomerated spherical particles of EAFD, the angular shape of OPC, and the needle-like shape of AC, as shown in Fig. 8e. The elemental composition of the mixture of 45 % EAFD doped with 2.0 % AC is provided, as shown in Fig. 8f. The primary elemental composition of the mixture consists of oxygen (O), carbon (C), iron (Fe), calcium (Ca), and zinc (Zn).

5.6. Specific surface area and pore size distribution

The specific surface area of all samples could be measured using the Brunauer-Emmett-Teller (BET) method. Table 6 displays the precise surface area of the EAFD replacement and the 45 % EAFD mixed with AC at the curing period of 28 days and w/b ratio of 0.40. The replacement of EAFD in the range of 0 %–50 % results in a specific surface area that ranges from 27.83 to 90.79 m^2/g. Replacing the specimen with EAFD results in an increase in the specific surface area of the specimen. Furthermore, replacing 45 % of EAFD with doped AC in the range of 0.5 %–2.0 % also led to an increase in the specific surface area. The increase in the specific surface area can be due to the higher hydration reaction. Sahar et al. discovered that an increase in the water/cement ratio leads to an increase in the specific surface area, which in turn enhances the hydration reaction and results in the formation of more pores [45]. Our research indicates that the concentration of EAFD and AC increases, resulting in a decrease in particle size and an increase in specific surface area, total pore volume, and average pore size. An increase in specific surface area is likely to have an impact on the hydration process, contributing to a slightly larger total pore volume and average pore size.

Fig. 9 displays the nitrogen adsorption-desorption isotherms of all samples. The loops observed in all samples were categorized as Type IV with a Type H1 hysteresis loop, based on the IUPAC classification of adsorption isotherms. The Type IV isotherm is a characteristic trait shown by materials containing mesoporous structures, which have pore sizes ranging from 2.0 to 50.0 nm. The Type H1 hysteresis loop is linked to porosity in agglomeration materials [46,47]. The pore size distribution was determined using the BJH method, revealing that the specimens had an average pore size ranging from 4.71 to 8.06 nm, with a total pore volume ranging from 0.06 to 0.15 nm, as shown in Table 6. The pore volume of all samples exhibited an increase with the addition of EAFD, which corresponded to a reduction in compressive strength. The BJH pore size distribution plot of all samples is shown in Fig. 10. The pore size distribution of all samples exhibited a consistent pattern. All samples have pore diameter ranging from 3.7 to 3.9 nm. With an increase

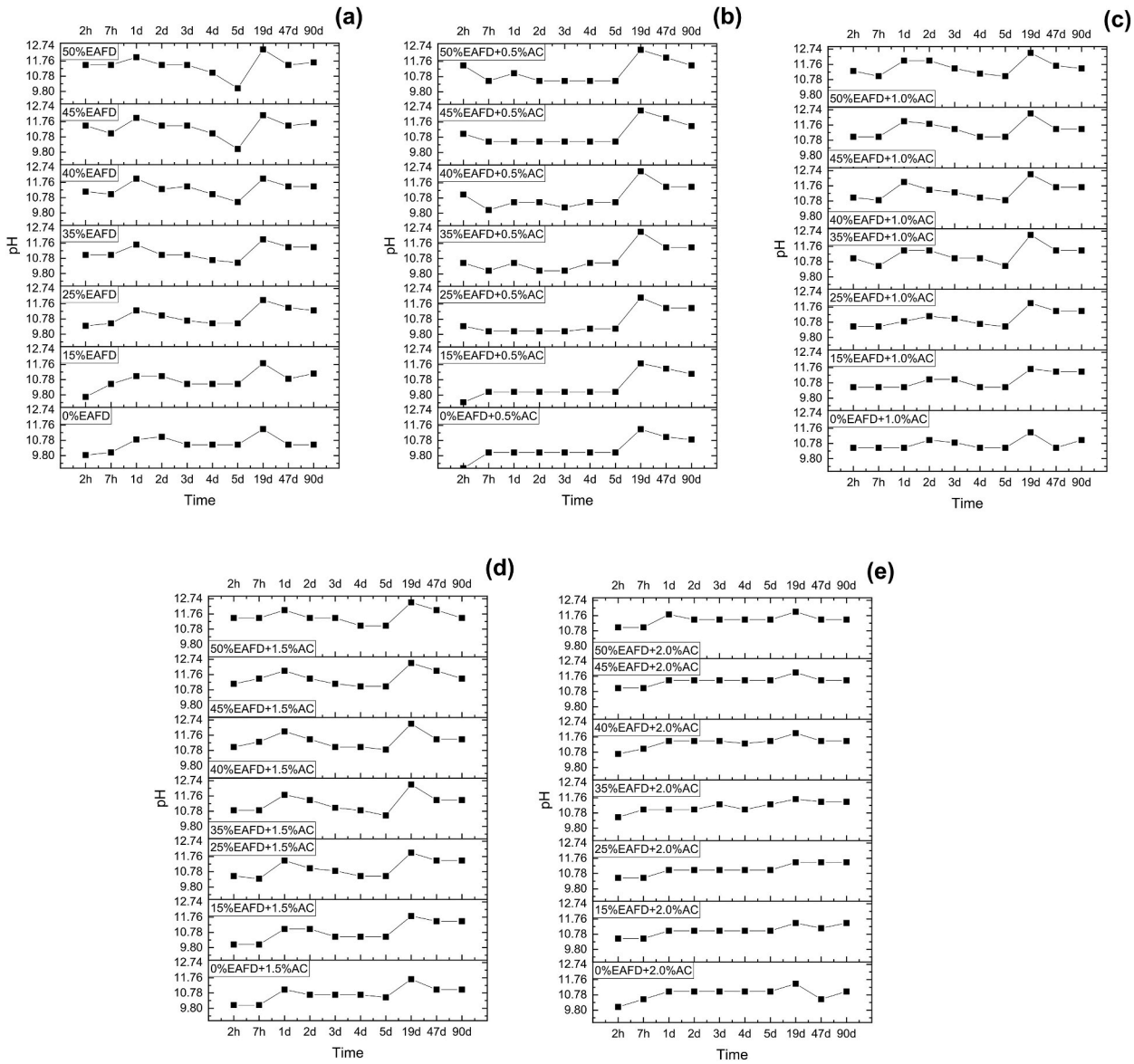

Fig. 6. The pH of leachate from different EAFD samples with varying amounts of AC doping: (a) 0 %, (b) 0.5 %, (c) 1.0 %, (d) 1.5 %, and (e) 2.0 %, over a period of 90 days.

in EAFD replacement concentration, the intensity of pore volume also increases. The rise in pore volume intensity suggests that the hydration reaction is high, resulting in the formation of pores [45].

6. Conclusions

The EAFD contaminated with Cs-137 was immobilized and doped with AC using the cementation technique. This study examined the strength and leaching behavior under various conditions. Based on the current study, the following conclusions can be determined:

- The compressive strength decreases as the quantity of EAFD increases, but increases with the reduction of water-to-binder ratios, the addition of AC, and longer curing time. The reduction in compressive strength is caused by the comparatively low quantities of C–S–H gel, $Ca(OH)_2$, and the formation of pores in the cementitious material, which take place during the hydration process.
- XRD result can confirm that the amount of $Ca(OH)_2$, which is produced during the hydration process, decreases as the quantity of EAFD rises, leading to a reduction in compressive strength.
- The SEM analysis indicated that the morphology of 45 % EAFD doped with 2.0 % AC exhibits more agglomeration and compaction compared to that of 45 % EAFD.

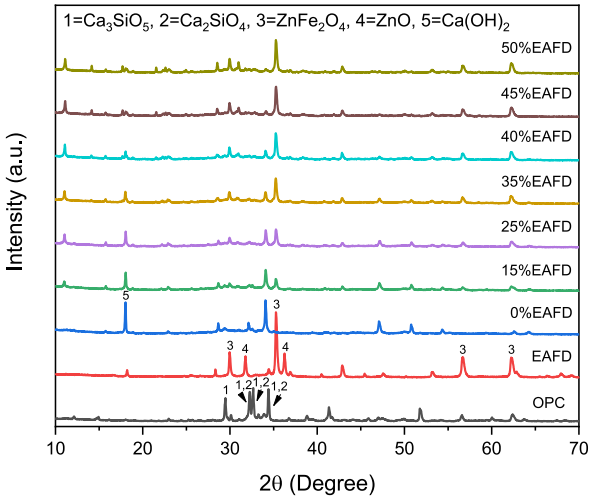

Fig. 7. The X-ray diffraction (XRD) patterns of OPC, EAFD, and the various replacements of EAFD.

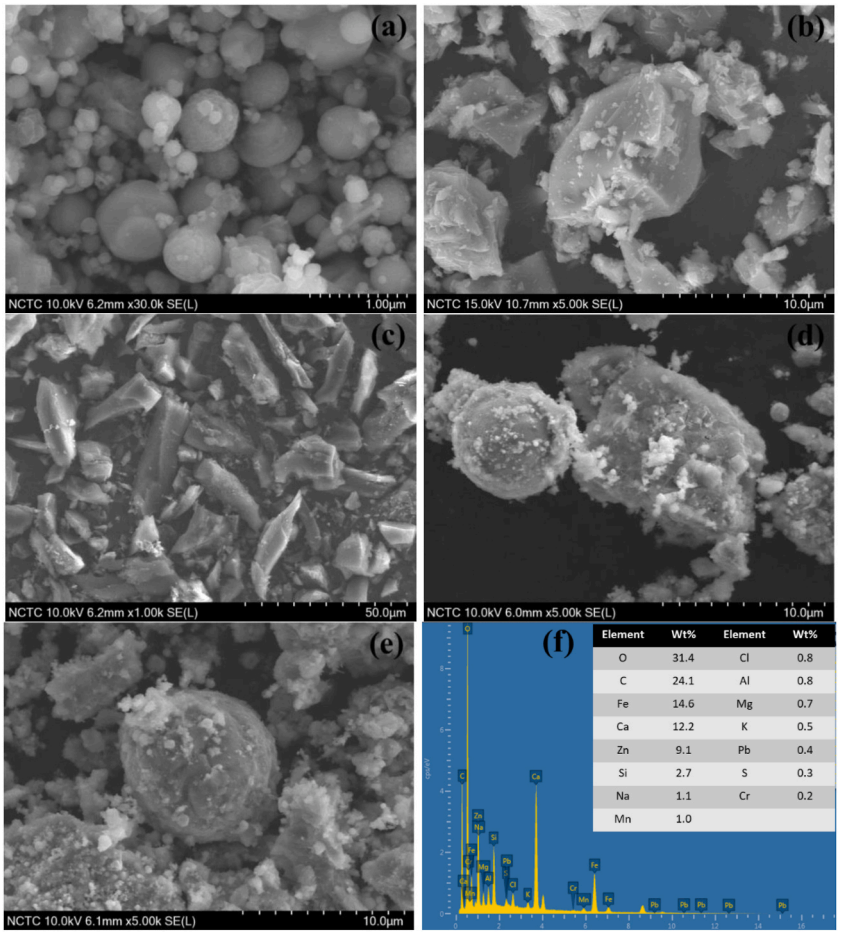

Fig. 8. SEM images of (a) electric arc furnace dust (EAFD), (b) ordinary Portland cement (OPC), (c) activated carbon (AC), (d) OPC-based 45 % EAFD, and (e–f) SEM-EDS of a mixture of 45 % EAFD doped with AC at a concentration of 2.0 %.

Table 6
BET surface area, total pore volume, and average pore diameter of the replacement of EAFD vary between 0 % and 50 %, and the 45 % of EAFD doped with AC ranging from 0.5 % to 2.0 % at the curing period of 28 days and w/b ratio of 0.40.

Samples	Specific surface area (m^2/g)	Total pore volume (cm^3/g)	Average pore size (nm)	Average particle size (nm)
OPC	ND	0.0078	53.69	ND
EAFD	8.79	0.04	16.17	682.96
AC	1205.05	0.72	5.00	4.98
0 % EAFD	27.83	0.06	8.06	215.63
15 % EAFD	63.67	0.09	4.71	94.23
25 % EAFD	88.75	0.12	4.51	67.60
35 % EAFD	90.79	0.13	4.74	66.09
40 % EAFD	87.08	0.13	5.07	68.91
45 % EAFD	70.75	0.11	5.05	84.81
50 % EAFD	72.60	0.11	4.88	82.64
45 % EAFD + 0.5 % AC	97.05	0.14	5.11	61.82
45 % EAFD + 1.0 % AC	99.95	0.15	5.38	60.03
45 % EAFD + 1.5 % AC	82.84	0.13	5.35	72.43
45 % EAFD + 2.0 % AC	93.98	0.14	5.30	63.84

*ND is not detected.

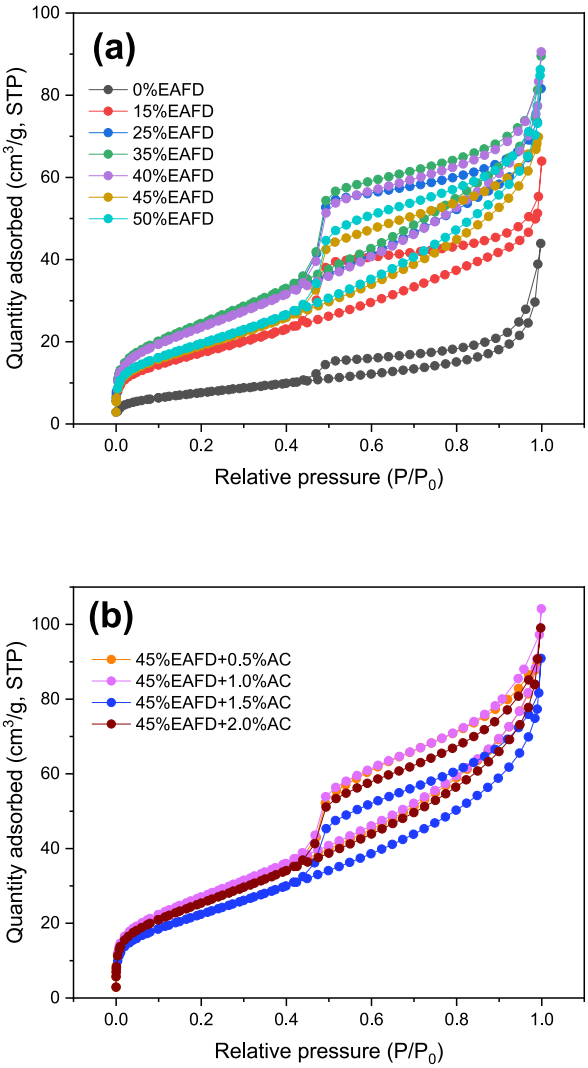

Fig. 9. The nitrogen adsorption-desorption isotherms for different samples: (a) OPC with varying proportions of EAFD and (b) the mixture of 45 % EAFD doped with AC at concentrations of 0.5 %, 1.0 %, 1.5 %, and 2.0 % by weight.

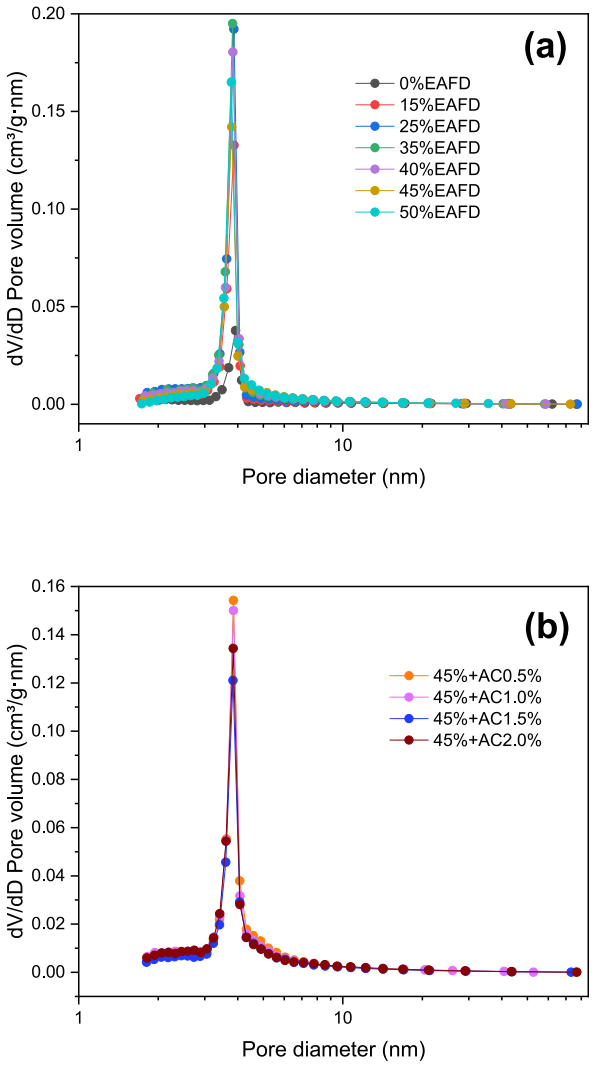

Fig. 10. The BJH desorption pore size distribution plots for different samples: (a) OPC with varying proportions of EAFD and (b) the mixture of 45 % EAFD doped with AC at concentrations of 0.5 %, 1.0 %, 1.5 %, and 2.0 % by weight.

- The BET and BJH study demonstrate that an increase in EAFD and AC concentration leads to a rise in specific surface area, total pore volume, and average pore size, which in turn results in a loss in compressive strength.
- The leaching test of the specimens was performed to assess the efficiency of immobilizing the radioactive Cs-137. The average LI values of all specimens range from 5.72 to 7.01, decreasing as the replacement of EAFD and AC concentrations increases.
- The leachates were analyzed to quantify the concentration of heavy metals during the final leaching test. During a 90-day period, the samples showed little leaching of heavy metal ions from EAFD, including aluminum (Al), cadmium (Cd), chromium (Cr), copper (Cu), iron (Fe), manganese (Mn), nickel (Ni), lead (Pb), and zinc (Zn). This can be attributed to the presence of effective barriers that hinder the movement of heavy metals and radioactive substances. Additionally, AC functions as a very efficient sorbent for the elimination of heavy metals and radionuclides.
- Our study findings indicate that a combination of 45 % EAFD and 1.5 % AC is suitable for effectively immobilizing EAFD contaminated with Cs-137. This choice takes into account the strength of the material, leaching properties, and waste capacity. The upcoming study will propose assessing the leaching examination across diverse environmental circumstances, comprising seawater, groundwater, and varying temperatures.

Data availability statement

Data included in article/supp. material/referenced in article.

CRediT authorship contribution statement

Sudarat Issarapanacheewin: Writing – review & editing, Writing – original draft, Visualization, Validation, Methodology, Investigation, Conceptualization. **Dechanun Choomjun:** Writing – original draft, Investigation. **Witsanu Katekaew:** Resources. **Nikom Prasertchiewchan:** Supervision. **Wilasinee Kingkam:** Investigation.

Declaration of competing interest

The authors declare that they have no known competing financial interests or personal relationships that could have appeared to influence the work reported in this paper.

Acknowledgements

The authors would like to acknowledge the financial support provided by Thailand Science Research and Innovation (Fundamental Fund, 2023, number 4368629) in conducting this research. We extend our appreciation to the Thailand Nuclear Technology Service Center, Thailand Institute of Nuclear Technology (Public Organization) for doing the XRF analysis. We express our gratitude to the Nuclear Technology Research and Development Center, Thailand Institute of Nuclear Technology (Public Organization) for doing the BET and BJH analysis. We would like to express appreciation to the Faculty of Science and Technology, Department of Applied Physics, Rajamangala University of Technology Thanyaburi for providing the porosity testing facility.

References

[1] J.A. De Araújo, V. Schalch, Recycling of electric arc furnace (EAF) dust for use in steel making process, J. Mater. Res. Technol. 3 (3) (2014) 274–279, https://doi.org/10.1016/j.jmrt.2014.06.003.
[2] S. Ahmad, W.R. Sajal, F. Gulshan, M. Hasan, M.A. Rhamdhani, Thermodynamic analysis of caustic–roasting of electric arc furnace dust, Heliyon 8 (10) (2022) e11031, https://doi.org/10.1016/j.heliyon.2022.e11031.
[3] M.C. Arnold, A.S. de Vargas, L. Bianchini, Study of electric-arc furnace dust (EAFD) in fly ash and rice husk ash-based geopolymers, Adv. Powder Technol. 28 (9) (2017) 2023–2034, https://doi.org/10.1016/j.apt.2017.05.007.
[4] A. Lozano-Lunar, P. Raposeiro da Silva, J. de Brito, J.M. Fernández, J.R. Jiménez, Safe use of electric arc furnace dust as secondary raw material in self-compacting mortars production, J. Clean. Prod. 211 (2019) 1375–1388, https://doi.org/10.1016/j.jclepro.2018.12.002.
[5] M. da Silva Magalhães, F. Faleschini, C. Pellegrino, K. Brunelli, Cementing efficiency of electric arc furnace dust in mortars, Construct. Build. Mater. 157 (2017) 141–150, https://doi.org/10.1016/j.conbuildmat.2017.09.074.
[6] E. Ordoñez, S. Neves Monteiro, H.A. Colorado, Valorization of a hazardous waste with 3D-printing: combination of kaolin clay and electric arc furnace dust from the steel making industry, Mater. Des. 217 (2022), https://doi.org/10.1016/j.matdes.2022.110617.
[7] F. Monroy-Guzmán, R.S. Juárez, M.D. Tenorio Castilleros, Recovery of Cs-137 from electric arc furnace dust by lixiviation, Case Stud. Chem. Environ. Eng. 6 (2022) 100234, https://doi.org/10.1016/j.cscee.2022.100234.
[8] J.Y. Goo, B.J. Kim, M. Kang, J. Jeong, H.Y. Jo, J.S. Kwon, Leaching behavior of cesium, strontium, cobalt, and europium from immobilized cement matrix, Appl. Sci. 11 (18) (2021), https://doi.org/10.3390/app11188418.
[9] K. Yubonmhat, T. Akharawutchayanon, P. Nuanjan, S. Issarapanacheewin, W. Katekaew, N. Prasertchiewchan, Progress and challenges of radioactive waste management in Thailand, J. Hazardous, Toxic, Radioact. Waste 26 (2) (2022) 1–14, https://doi.org/10.1061/(asce)hz.2153-5515.0000693.
[10] R.O. Abdel Rahman, A.A. Zaki, Comparative analysis of nuclear waste solidification performance models: spent ion exchanger-cement based wasteforms, Process Saf. Environ. Prot. 136 (2020) 115–125, https://doi.org/10.1016/j.psep.2019.12.038.
[11] P. Szajerski, Solidification of radioactive waste in lignite slag and bismuth oxide filled elastomer matrices: release mechanism, immobilization efficiency, long term radiation stability and aging, Chem. Eng. J. 404 (July 2020) (2021), https://doi.org/10.1016/j.cej.2020.126495.
[12] J. Li, L. Chen, J. Wang, Solidification of radioactive wastes by cement-based materials, Prog. Nucl. Energy 141 (May) (2021) 103957, https://doi.org/10.1016/j.pnucene.2021.103957.
[13] J.H. Kim, E.A. Seo, D.G. Kim, C.W. Chung, Utilization of recycled cement powder as a solidifying agent for radioactive waste immobilization, Construct. Build. Mater. 289 (2021) 123126, https://doi.org/10.1016/j.conbuildmat.2021.123126.
[14] K. Yubonmhat, P. Gunhakoon, P. Sopapan, N. Prasertchiewchan, W. Katekaew, Ordinary-Portland-cement solidification of Cs-137 contaminated electric arc furnace dust from steel production industry in Thailand, Heliyon 10 (3) (2024) e25792, https://doi.org/10.1016/j.heliyon.2024.e25792.
[15] H.M. Saleh, H.R. Moussa, F.A. El-Saied, M. Dawoud, T.A. Bayoumi, R.S. Abdel Wahed, Mechanical and physicochemical evaluation of solidified dried submerged plants subjected to extreme climatic conditions to achieve an optimum waste containment, Prog. Nucl. Energy 122 (2020) 1–11, https://doi.org/10.1016/j.pnucene.2020.103285.
[16] H.M. Saleh, S.M. El-Sheikh, E.E. Elshereafy, A.K. Essa, Mechanical and physical characterization of cement reinforced by iron slag and titanate nanofibers to produce advanced containment for radioactive waste, Construct. Build. Mater. 200 (2019) 135–145, https://doi.org/10.1016/j.conbuildmat.2018.12.100.
[17] H.M. Saleh, I.I. Bondouk, E. Salama, H.H. Mahmoud, K. Omar, H.A. Esawii, Asphaltene or polyvinylchloride waste blended with cement to produce a sustainable material used in nuclear safety, Sustainability 14 (2022) 1–14, https://doi.org/10.3390/su14063525.
[18] I. Nikolic, et al., Alkali activated slag cement doped with Zn-rich electric arc furnace dust, J. Mater. Res. Technol. 9 (6) (2020) 12783–12794, https://doi.org/10.1016/j.jmrt.2020.09.024.
[19] C. Shi, A. Fernández-Jiménez, Stabilization/solidification of hazardous and radioactive wastes with alkali-activated cements, J. Hazard Mater. 137 (3) (2006) 1656–1663, https://doi.org/10.1016/j.jhazmat.2006.05.008.
[20] E.F. Ledesma, A. Lozano-Lunar, J. Ayuso, A.P. Galvín, J.M. Fernández, J.R. Jiménez, The role of pH on leaching of heavy metals and chlorides from electric arc furnace dust in cement-based mortars, Construct. Build. Mater. 183 (2018) 365–375, https://doi.org/10.1016/j.conbuildmat.2018.06.175.
[21] E.F. Ledesma, J.R. Jiménez, J. Ayuso, J.M. Fernández, J. de Brito, Experimental study of the mechanical stabilization of electric arc furnace dust using fluid cement mortars, J. Hazard Mater. 326 (2017) 26–35, https://doi.org/10.1016/j.jhazmat.2016.11.051.
[22] A.V. Makarov, et al., Activated carbon additives for technetium immobilization in bentonite-based engineered barriers for radioactive waste repositories, J. Hazard Mater. 401 (June) (2021) 123436, https://doi.org/10.1016/j.jhazmat.2020.123436.
[23] P. Sopapan, et al., Management of 137Cs in electric arc furnace dust by solid-liquid extraction and treatment of contaminated wastewater using co-precipitation, Case Stud. Chem. Environ. Eng. 7 (December 2022) (2023) 100283, https://doi.org/10.1016/j.cscee.2022.100283.
[24] P. Sopapan, et al., Effective removal of non-radioactive and radioactive cesium from wastewater generated by washing treatment of contaminated steel ash, Nucl. Eng. Technol. 55 (2) (2023) 516–522, https://doi.org/10.1016/j.net.2022.10.007.
[25] T. Akharawutchayanon, et al., Removal efficiency of 137Cs from radioactively contaminated electric arc furnace dust using different solvents, Case Stud. Chem. Environ. Eng. 8 (May) (2023) 100409, https://doi.org/10.1016/j.cscee.2023.100409.

[26] Z. Laili, M.S. Yasir, M.A.W. Yusof, Leaching behaviour of Cs-134 immobilised in cement-biochar matrix, J. Teknol. 78 (7) (2016) 59–67, https://doi.org/10.11113/jt.v78.6296.
[27] R.O. Abdel Rahman, A.A. Zaki, Assessment of the leaching characteristics of incineration ashes in cement matrix, Chem. Eng. J. 155 (3) (2009) 698–708, https://doi.org/10.1016/j.cej.2009.09.002.
[28] American Nuclear Society, *ANSI/ANS-16.1-2003 (R2008) American national standard Measurement of the Leachability of solidified low-level radioactive Wastes by a short-term test procedure*. 555 north kensington avenue La grange park. Illinois 60526 USA Approved, American Nuclear Society, 2003.
[29] J. Shon, H. Lee, G. Kim, T. Kim, B. Ahn, Evaluation of disposal stability for cement solidification of lime waste, Materials 15 (3) (2022) 1–13, https://doi.org/10.3390/ma15030872, 872.
[30] A. Akyıldız, E.T. Köse, A. Yıldız, Compressive strength and heavy metal leaching of concrete containing medical waste incineration ash, Construct. Build. Mater. 138 (2017) 326–332, https://doi.org/10.1016/j.conbuildmat.2017.02.017.
[31] S. Kashef-Haghighi, Y. Shao, S. Ghoshal, Mathematical modeling of CO2 uptake by concrete during accelerated carbonation curing, Cement Concr. Res. 67 (October) (2015) 1–10, https://doi.org/10.1016/j.cemconres.2014.07.020.
[32] A. AlKhatib, M. Maslehuddin, S.U. Al-Dulaijan, Development of high performance concrete using industrial waste materials and nano-silica, J. Mater. Res. Technol. 9 (3) (2020) 6696–6711, https://doi.org/10.1016/j.jmrt.2020.04.067.
[33] M. Castellote, E. Menéndez, C. Andrade, P. Zuloaga, M. Navarro, M. Ordóñez, Radioactively contaminated electric arc furnace dust as an addition to the immobilization mortar in low-and medium-activity repositories, Environ. Sci. Technol. 38 (10) (2004) 2946–2952, https://doi.org/10.1021/es034518p.
[34] M.A. Uddin, M. Jameel, H.R. Sobuz, N.M.S. Hasan, M.S. Islam, K.M. Amanat, The effect of curing time on compressive strength of composite cement concrete, Appl. Mech. Mater. 204–208 (October) (2012) 4105–4109, 10.4028/www.scientific.net/AMM.204-208.4105.
[35] H.M. Saleh, F.A. El-Saied, T.A. Salaheldin, A.A. Hezo, Influence of severe climatic variability on the structural, mechanical and chemical stability of cement kiln dust-slag-nanosilica composite used for radwaste solidification, Construct. Build. Mater. 218 (2019) 556–567, https://doi.org/10.1016/j.conbuildmat.2019.05.145.
[36] N. Samson, A. Aondowase, J. Shiwua, Effect of Water-Cement Ratio on the Compressive Strength of gravel - crushed over burnt bricks concrete, Civ. Environ. Res. 3 (4) (2013) 74–82.
[37] S. Na, S. Lee, S. Youn, Experiment on activated carbon manufactured from waste coffee grounds on the compressive strength of cement mortars, Symmetry (Basel). 13 (2021) 1–9, https://doi.org/10.3390/sym13040619.
[38] Y. Wang, Y. Ge, X. Wang, X. Chen, Q. Li, The effect of powder activated carbon on mechanical properties and pore structures of cement-based mortars, Construct. Build. Mater. 316 (2022) 125798, https://doi.org/10.1016/j.conbuildmat.2021.125798.
[39] C. Zheng, Z. Liu, J. Xu, X. Li, Y. Yao, Compressive strength and microstructure of activated carbon-fly ash cement composites, Chem. Eng. Trans. 59 (2017) 475–480, https://doi.org/10.3303/CET1759080.
[40] H.M. Saleh, A.A. Salman, A.A. Faheim, A.M. El-Sayed, Influence of aggressive environmental impacts on clean, lightweight bricks made from cement kiln dust and grated polystyrene, Case Stud. Constr. Mater. 15 (2021) 1–16, https://doi.org/10.1016/j.cscm.2021.e00759.
[41] Y.F. Su, et al., Autogenous healing performance of internal curing agent-based self-healing cementitious composite, Cem. Concr. Compos. 114 (January) (2020), https://doi.org/10.1016/j.cemconcomp.2020.103825.
[42] Z. Laili, M.S. Yasir, M.A. Wahab, Solidification of radioactive waste resins using cement mixed with organic material, AIP Conf. Proc. 1659 (April 2015, 2015), https://doi.org/10.1063/1.4916876.
[43] D. Smržová, et al., Carbon and zeolite-based composites for radionuclide and heavy metal sorption, Heliyon 8 (12) (2022) e12293, https://doi.org/10.1016/j.heliyon.2022.e12293.
[44] H. Zhao, M. Deng, M. Tang, A comparative study on cement hydration and microstructure of cement paste incorporating aminosulfonate-phenol-salicylic acid-formaldehyde and aminosulfonate-phenol-formaldehyde polymer, J. Therm. Anal. Calorim. 112 (3) (2013) 1465–1474, https://doi.org/10.1007/s10973-012-2703-x.
[45] S. Seifi, D. Levacher, A. Razakamanantsoa, N. Sebaibi, Microstructure of dry mortars without cement: specific surface area, pore size and volume distribution analysis, Appl. Sci. 13 (9) (2023), https://doi.org/10.3390/app13095616.
[46] W. Kingkam, S. Issarapanacheewin, S. Nuchdang, P. Pakawanit, V. Puripunyavanich, D. Rattanaphra, Experimental investigation on biodiesel production through simultaneous esterification and transesterification using mixed rare earth catalysts, Energy Rep. 8 (2022) 857–870, https://doi.org/10.1016/j.egyr.2022.10.169.
[47] B. Mallesham, A. Rangaswamy, B.G. Rao, T.V. Rao, B.M. Reddy, Solvent-free production of glycerol carbonate from bioglycerol with urea over nanostructured promoted SnO2 catalysts, Catal. Lett. 150 (12) (2020) 3626–3641, https://doi.org/10.1007/s10562-020-03241-9.